Experimental investigation and theoretical modeling of textured silicon solar cells with rear metallization

A.V. Sachenko[1], V.P. Kostylyov[1*], R.M. Korkishko[1], V.M. Vlasiuk[1], I.O. Sokolovskyi[1], M. Evstigneev[2], O.Ya. Olikh[3], A.I. Shkrebtii[4*], and D. Johnston[5]

[1] V. Lashkaryov Institute of Semiconductor Physics, NAS of Ukraine, 03028 Kyiv, Ukraine

[2] Department of Physics and Physical Oceanography, Memorial University of Newfoundland, St. John's, NL, A1B 3X7, Canada

[3] Taras Shevchenko National University of Kyiv, 01601 Kyiv, Ukraine

[4] Ontario Tech University, Oshawa, ON, L1G 0C5, Canada

[5] Florida Gulf Coast University, Fort Myers, Florida 33913, USA

[*]Corresponding authors: Anatoli.Chkrebtii@ontariotechu.ca, vkostylyov@ukr.net

Abstract

Crystalline Silicon (c-Si) remains a dominant photovoltaics material in solar cell industry. Currently, scientific and technological advances make possible of producing the c-Si solar cells (SCs) efficiency close to the fundamental limit. Therefore, combining the experimental results and the modeling becomes crucial to further progress in improving the efficiency and reducing the photovoltaics systems cost. We carried out the experimental characterization of the highly-efficient c-Si SCs and compared with the modeling. For this purpose, we developed and applied to the samples under investigation the improved theoretical model to optimize characteristics of highly efficient textured solar cells. The model accounts for all recombination mechanisms, including nonradiative exciton recombination and recombination in the space-charge region (SCR). To compare the theoretical results with an experiment, we proposed empirical formula for the external quantum efficiency (EQE), which describes its experimental spectral dependence near the absorption edge. The approach proposed allows modeling of the short-circuit current and photoconversion efficiency in the textured crystalline silicon solar cells. The theoretical results, compared to the experimental measurements, allowed to validate the formalism developed, and were used to optimize the key parameters of the SCs, such as the base thickness, doping level and others.

Keywords— silicon, solar cell, texture, efficiency, recombinations, optimization

I. INTRODUCTION

Today, solar panels, made using polycrystalline and crystalline silicon, dominate the photovoltaic market, contributing to more than 90% of the global solar energy production [1], [2]. The current efficiency record of c-Si solar cells is 26.7% [3,4] against an intrinsic limit of 29.7% [5]. The efforts of scientists and engineers in the field, on one hand, are aimed at further enhancing the efficiency of SCs photoconversion, and, on the other, at reducing a cost of solar panels. High-performance crystalline silicon-based solar cells with an efficiency of 20% and above are based on $p - n$ junctions or heterojunctions with very thin layers of amorphous hydrogenated silicon SCs [3],[4], [6]. Such SCs have several features in common: first, their top or both top and bottom surfaces are textured, which significantly reduces reflection of the incident light and enhances the light trapping. To increase the SCs energy output by maximizing their photoconversion efficiency η, surface texturing techniques are developed to reduce the optical reflection losses and maximize the light absorbed. Therefore, surface texturing of silicon photovoltaics systems currently is drawing much attention [2], [6] [7] . The second common feature is that the Shockley-Reed-Hall (SRH) lifetime, responsible for the recombination in the bulk, is several milliseconds and the diffusion length of excess charge carriers is much longer than SC thickness. Currently, further increase of the silicon SC efficiency becomes more and more difficult, and requires better consideration of the physical processes in the SCs. In particular, to further increase the SCs efficiency it is necessary to take into account all contributing recombination mechanisms in silicon. This has to include a non-radiative exciton recombination via deep impurity centers [8] and recombination in the space-charge region (SCR) [9] . Still, the above two mechanisms are not included in the existing SC optimization formalisms and software [10]. However, as we previously demonstrated [11], these recombination processes are detrimental in the high-efficiency silicon-based SCs. They may significantly influence the SCs efficiency as compared to the mechanisms that are already considered, such as, in particular, the radiative and band-to-band Auger recombinations.

Particularly challenging are calculations of the absorption and external quantum efficiency of the textured silicon SCs. Even though the existing optimization software packages are advanced enough, they do not provide the unique solution of the problem of the thickness optimization for the textured SCs. However, in one of our papers [12] we offered a solution of the problem by introducing a simple empirical formula for calculating the external quantum efficiency, which allows to successfully overcome the problems with the absorption and external quantum efficiency that the available formalisms suffer.

Therefore, to advance in improvement of the SCs efficiency, the available optimisation approaches should be further developed and applied to highly efficient SCs, which is the goal of the paper. In order to model and optimize textured high-efficiency silicon SCs we first measured and analyzed the experimental

dependencies of the external quantum efficiency (EQE). Next, we calculated the short-circuit current and the photoconversion efficiency under AM1.5 conditions, which are dependent on the SC base thickness *d* and its doping level. The results were applied to optimize characteristics of the textured silicon SCs, using a concept a completely randomized Lambert surface [13], which is the commonly accepted model for surface texturing from the reflection reduction point of view. However, we stress that the theoretical approach presented is applicable to any arbitrary textured SCs surface and all the main types of silicon-based high efficiency textured SCs.

The presented self-consistent approach for the textured Si solar cells efficiency η has been validated experimentally. Dark and light *I–V* characteristics as well as light intensity dependence of the open-circuit voltage were measured for a number of highly efficient silicon *p-n* junction SCs with the photoconversion efficiency $\eta \geq 20\%$. The important component of the formalism, namely spectral dependencies of $EQE(\lambda)$ under AM1.5 conditions were also investigated experimentally.

For the textured silicon SCs considered, the experimental dependencies of *EQE(λ)* were analyzed. It is shown that close to the absorption edge *EQE(λ)* dependence can be accurately described by the empirical formula with a variable parameter, dependent on the SC. Using the experimental *EQE(λ)* dependence, represented by the proposed formula, we calculated the dependence of the short-circuit current density J_{SC} on the base thickness *d* for the textured SCs.

In the calculations and comparison of the theory with the experiment, in addition to the radiative and Auger recombinations we also considered nonradiative exciton recombination by the Auger mechanism via a deep recombination center [14] and recombination in the space charge region (SCR) [15].

The paper is organized as following. We describe first in the section II the experimental details and the recombination mechanisms in the silicon-based SCs considered. In the section III we offer the optimization formalism description. Experimental results, compared to the simulations, will be presented in the section IV. Section V offers the summary of the research.

II. TECHNICAL DETAILS AND MAIN PARAMETERS

Dark volt-ampere *(I–V)* characteristics were measured on samples of high-efficiency SCs ($\eta \geqslant 20\%$) using an external source of stable voltage. The short-circuit current density J_{sc} dependence on the open-circuit voltage V_{os} was measured in a wide incoming irradiance range of $10 \div 1200$ W/m^2 using a set of attenuating filters. Light *I–V* characteristics were measured under the AM1.5G conditions (1000W/m^2) at 25°C using Newport Oriel KSH-7320 ABA MiniSol Solar Simulator; Newport 91150V Reference PV Cell kit; Keithley 2400 Source Meter to measure cell *I-V* characteristics; LabView Software to automate testing. The spectral dependencies of the external quantum efficiency *EQE(λ)* were measured in the wavelength

range $\Delta\lambda$ of 360 ÷1200 nm with the grating monochromator using the SCs short-circuit mode, automatically maintaining constant flux of the monochromatic photons at a specified level. For this, the photon flux was divided, using the oscillating beam splitter with a frequency of 20 Hz, into the channel for maintaining the photon flux at a given constant level and into the channel for measuring the external quantum efficiency of the sample under investigation. In this case, the photon flux was modulated with a frequency of 20 Hz. The amplification on an alternating signal with a frequency of 20 Hz, followed by a lock-in amplifier, improved the signal-to-noise ratio.

To demonstrate the application of the formalism by comparing the experimental results and the theory, we characterize experimentally the back junction back contact solar cells, also called interdigitated back contact solar cells (IBC SCs)). In particular, we measured characteristics of the commercial textured silicon *p-n* junction SCs with a photoconversion efficiency η above 21%, which are manufactured by SunPower™.

For the modelling and optimization of the photo-conversion efficiency of the SC in terms of base thickness *d* and the doping level *n* the analytical expression for $EQE(\lambda)$. We established that the experimental spectral dependencies of the external quantum efficiency $EQE(\lambda)$ in textured silicon SCs near the absorption edge can be described by an empirical formula $EQE(\lambda)=[1+b/(4n_r(\lambda)^2\cdot\alpha(\lambda)d)]^{-1}$, where $\alpha(\lambda)$ is the light absorption coefficient, *d* is the base thickness, n_r is the refractive index, and *b* is a non-dimensional coefficient, which characterizes the texturing quality, and ranging from 1.6 to 4. It is usually greater than 1, when b=1 the established empirical formula transforms into the well-known Yablonovitch formula [16] for absorbance. Physical meaning of the parameter *b* is the ratio of the photon path length in the case of a perfectly randomized surface, considered in [13], to the photon path length in a particular sample with a nonrandomized surface.

Fig. 1 shows the experimental external quantum efficiency $EQE(\lambda)$, measured, for the SunPower™ IBC SC investigated, compared with that one from the empirical formula, the parameter b = 4 was used.

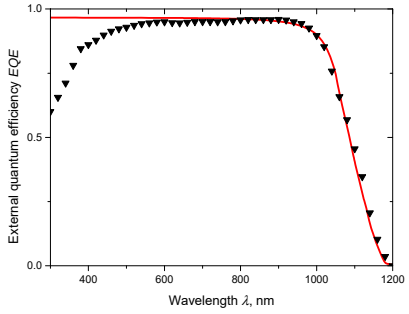

Fig. 1. Experimental (triangles) and theoretical (calculated by the empirical formula, red line) dependencies of $EQE(\lambda)$ for SunPower™ IBC SC under investigation.

The minority carrier lifetime τ is one of the most important parameters for the characterization of semiconductor, used in SCs [17]. The total effective recombination time τ_{eff}, which includes all recombination mechanisms, can be written as:

$$\tau_{eff}(n) = \left[\frac{1}{\tau_{SRH}(n)} + \frac{1}{\tau_{nr}(n)} + \frac{S_{0S}}{d}\left(1 + \frac{\Delta n}{n_0}\right) + \frac{1}{\tau_r(n)} + \frac{1}{\tau_{Auger}(n)} + \frac{S_{SC}(n)}{d}\right]^{-1}, \quad (1)$$

where $n = n_0 + \Delta n$ is the total concentration of the majority carries (electrons, for definiteness) with the equilibrium concentration, with n_0 is the base doping level, and Δn is the excess concentration of the electron-hole pairs (EHPs). $S_{0S} = S_{00} + S_{0d}$ is the total surface recombination velocity at the front and back surfaces of the solar cell in the low-injection regime, $\tau_{nr}(n) = \tau_{SRH} \cdot \left(\frac{n_x}{n}\right)$ is the nonradiative exciton recombination time [8], $\tau_r(n)$ is the radiative recombination time [4], $\tau_{Auger}(n)$ is the Auger interband recombination time [18], and S_{sc} is recombination rate in the SCR.

The Shockley–Read–Hall (SRH) recombination time τ_{SRH} for n-type Si can be written as:

$$\tau_{SRH}(n) \cong \frac{\tau_{p0}(n_0+\Delta n+n_1)+\tau_{n0}(p_1+\Delta n)}{(n_0+\Delta n)}, \quad (2)$$

where $\tau_{p0} = \left(C_p N_t\right)^{-1} s$ and $\tau_{n0} = (C_n N_t)^{-1} s$, with the hole (electron) capture coefficient C_p (C_n) by the recombination centers with concentration N_t, while n_1 and p_1 denote respectively the electron and hole densities, when the Fermi level coincides with the trap level, the so-called Shockley-Reed factors for electrons and holes.

Note that the Shockley-Reed-Hall lifetime τ_{SRH} depends on the recombination center location inside the gap and the capture coefficient for electrons and holes. With increasing doping level and excitation level the lifetime generally changes in the range between two values, and it can increase, decrease or remain practically constant. In the following we consider that τ_{SRH} is constant in the standard range of the doping levels and excitation (for the EHP excess concentration in the range from 10^{14} to 10^{16} cm^{-3}).

The expression for the radiative recombination lifetime can be written as [4]:

$$\tau_{rad}^{-1} = B_r\ (1 - P_{PR})\ (n_0 + \Delta n)\ , \quad (3)$$

where B_r is the radiative recombination parameter in silicon, and P_{PR} is the probability of photon reabsorption. Following [4], the expression for B_r is:

$$B_r = \int_0^\infty dE\ B(E), \qquad \text{with } B(E) = \left(\frac{n_r(E)\ \alpha(E)\ E}{\pi\ c\ \hbar^{\frac{3}{2}}\ n_i}\right)^2 e^{-\frac{E}{k_B T}}. \tag{4}$$

Here $n_r(E)$ is the silicon refractive index, $\alpha(E)$ is the photon energy dependent absorption coefficient, and $E = \frac{hc}{\lambda}$.

The probability of photon reabsorption in the SC base can be defined as:

$$P_{PR} = B^{-1} \int_0^\infty dE\ A_{bb}(E)\ B(E)\,, \tag{5}$$

with the absorbance $A_{bb}(E)$ equals to

$$A_{bb}(E) = \frac{\alpha}{\alpha + \frac{b}{4n_r^2 d}}. \tag{6}$$

Expression (6) differs from that one from [16] in that it introduces a coefficient b greater than 1. As for the interband recombination lifetime $\tau_{Auger}(n)$, the empirical expression given in [18] is used.

The expression for the recombination rate in SCR S_{nr} is usually derived under the assumption that it occurs via a deep level, close to the middle of the band gap, and for the case of silicon it was presented and analyzed in [19], [20]. This was done in the model, when the discrete bulk deep level with the energy E_t is close to the middle of the band gap, with the concentration N_t^* and the capture cross sections of electron and hole σ_n and σ_p.

We used the following expression to calculate the recombination rate S_{nr} in the SCR (see [9], [21]):

$$S_{nr}(\Delta n) = \int_0^w \frac{(n_0+\Delta n)dx}{\left[\left((n_0+\Delta n)e^{y(x)} + n_i(T)\ exp\left(\frac{E_t}{kT}\right)\right) + b_r\left((p_0+\Delta n)e^{-y(x)} + n_i(T)\ exp\left(-\frac{E_t}{kT}\right)\right)\cdot \tau_R(x)\right]}. \tag{7}$$

Here $b_r = \frac{C_p}{C_n}$, $C_n = V_{nT}\sigma_n$, $C_p = V_{pT}\sigma_p$, with the average thermal velocities of electrons and holes V_{nT} and V_{pT}, $\tau_R(x) = (C_p N_t^*(x))^{-1}$ is the EHP lifetime in the SCR, N_t^* is the deep level concentration in the SCR, p_0 is the equilibrium bulk hole concentration, $y(x)$ is the dimensionless electrostatic potential in the SCR, E_t is the energy of the deep level in the silicon SCR, calculated from the middle of the gap, $n_i(T)$ is the concentration of intrinsic charge carriers, and w is the SCR thickness.

To find the nonequilibrium dimensionless potential $y(x)$, we solve the second order integral Poisson equation in the following form:

$$x = \int_{y_0}^{y} \frac{L_D}{\left[\left(1+\frac{\Delta n}{n_0}\right)(e^{y_1}-1) - y_1 + \frac{\Delta n}{n_0}(e^{-y_1}-1)\right]^{0.5}} dy_1, \tag{8}$$

where $L_D = \left(\frac{\varepsilon_0 \varepsilon_{Si} kT}{2q^2 n_0}\right)^{\frac{1}{2}}$ is the Debye length, and q is the elementary charge.

The nonequilibrium dimensionless potential y_0 at x=0 can be found by solving the electroneutrality equation [19] in the form:

$$N = \pm\left(\frac{2kT\varepsilon_0\varepsilon_{Si}}{q^2}\right)^{\frac{1}{2}}[(n_0 + \Delta n)(e^{y_0} - 1) - n_0 y_0 + \Delta n(e^{-y_0} - 1)]^{\frac{1}{2}}, \quad (9)$$

where qN is the acceptors surface charge density in the p-n junction or anisotype heterojunction.

From Eq. (8) we obtain the following expression for the SCR thickness w:

$$w = \int_{y_0}^{y_w} \frac{L_D}{\left[\left(1+\frac{\Delta n}{n_0}\right)(e^{y}-1) - y + \frac{\Delta n}{n_0}(e^{-y}-1)\right]^{0.5}} dy, \quad (10)$$

where y_w is the nonequilibrium dimensionless potential at the boundary between the SCR and the quasi-neutral bulk.

Using the expressions (7) - (10), the S_{nr} dependence on the electron-hole pairs excess density Δn can be calculated.

Let's analyze the case when the lifetime in the SCR τ_R is small compared to the bulk lifetime, and τ_R is constant inside the space charge region d_0, in which the nonequilibrium dimensionless potential modulus is less than one. Always, d_0 is less than the SCR width at the equilibrium w and much smaller than the base width d. If Δn is small enough ($\Delta n \ll n_0$), we obtain from (7) the recombination rate S_{sc} in the SCR. For the limit of large Δn ($\Delta n) n_0$) we can define the recombination rate $\frac{d_0}{\tau_R}$, in the layer with a small lifetime τ_R. This occurs when the absolute value of the nonequilibrium dimensionless potential at the boundary of n and p^+ layer is less than one, that is the bands are almost completely flattened. In the intermediate cases, we obtain from (7) a sum of the recombination rates in the SCR S_{SC} and $\frac{d_0 - w(\Delta n)}{\tau_R}$, where $w(\Delta n)$ is the SCR thickness for a given Δn.

In the case when the lifetime in the SCR equals to that one of the bulk, this will not be the case. Since $w(\Delta n = 0) << d$, the addition to the bulk recombination rate due to the bands flattening $\frac{w(\Delta n < n_0)}{\tau_b}$, ($\tau_b$ is the bulk lifetime) will be very small compared to the bulk recombination rate and can always be neglected.

What happens if the typical silicon SCs parameters are used in the calculations? In the approximation of a constant SCR lifetime τ_r, the calculated slope of $S_{sc}(\Delta n)$ is higher than the experimental one, and agreement between the theory and experiment is not achieved when $\Delta n \ll n_0$ for the small lifetime values,

no matter what the base thickness is. A much better agreement between the experiment and the theory can be achieved assuming the Gaussian distribution of the inverse life time in the SCR:

$$\tau_R{}^{-1}(x) = \tau_m^{-1}\, exp\left(\frac{-(x-x_m)^2}{2\sigma^2}\right), \tag{11}$$

where τ_m is the life time at the point of maximum, x_m is a position of the maximum, and σ is the dispersion.

In this case $S_{sc}(\Delta n) \equiv S_{nr}(\Delta n)$, and by reducing the half-width of the gaussian, a faster decrease of $S_{sc}(\Delta n)$ can be achieved. Sufficiently large values of $S_{sc}(\Delta n)$ for small Δn can be achieved by reducing the lifetime τ_m.

Note that for the SCs with rear contact metallization, recombination in the SCR does not occur over the entire SC area A_{SC}. It happens only in the places where inversion band bending occurs, that is in the area, doped with boron, with its surface A_B less than A_{SC}. Therefore, for this case in the expression (1) for τ_{eff} it is necessary to write $S_{SC}\cdot\left(\frac{A_B}{A_{SC}}\right)$ instead of S_{SC}.

III. PHOTOCONVERSION EFFICIENCY FORMALISM

The light *I-V* characteristics for the rear contact metallization solar cells (RC SCs) under consideration (they are also called interdigitated back contact solar cells (IBC SCs)) were calculated using the expressions from [8], [15], [18]:

$$I(V) = I_L - \frac{qA_{SC}d\ \Delta n}{\tau_{eff}(\Delta n)} - \frac{V+IR_s}{R_{sh}} \tag{12}$$

$$I_r(V) = qA_{SC}\left(\frac{d}{\tau_{eff}^b} + S_{00s}\left(1+\frac{\Delta n}{n_0}\right) + \frac{A_B}{A_{SC}}S_{sc}\right)\Delta n(V), \tag{13}$$

$$\tau_{eff}^b(n) = \left[\frac{1}{\tau_{SRH}} + \frac{1}{\tau_r(n)} + \frac{1}{\tau_{nr}(n)} + \frac{1}{\tau_{Auger}(n)}\right]^{-1}, \tag{14}$$

$$\Delta n(V) = -\frac{n_0}{2} + \sqrt{\frac{n_0^2}{4} + n_{i0}(T)^2 e^{\frac{\Delta E_g}{kT}}\left(exp\frac{q(V-IR_s)}{kT} - 1\right)}, \tag{15}$$

where $I(V)$ is the total current, I_L is the photogeneration current, $I_r(V)$ is recombination (dark) current, V is applied voltage, $\tau_{eff}^b(n)$ is effective bulk lifetime, R_s and R_{SH} are series and shunt resistances, n_{i0} is the intrinsic concentration at low injection [22], and $\Delta E_g(n_0,\Delta n)$ is the magnitude of bandgap narrowing in Si [18].

The expression for the dark current according to (12) has the form:

$$I_D(V) = \frac{qA_{SC}d\ \Delta n}{\tau_{eff}(\Delta n)} + \frac{V-I_DR_s}{R_{sh}}. \tag{16}$$

The photogeneration current I_L dependence on the open circuit voltage V_{OC} can be found from (12) by putting $I = 0$:

$$I_L = \frac{A_{SC} q d}{\tau_{eff}(\Delta n_{OC})} \Delta n_{OC} + \frac{V_{OC}}{R_{sh}}, \tag{17}$$

with

$$\Delta n_{OC} = -\frac{n_0}{2} + \sqrt{\frac{n_0^2}{4} + n_{i0}^2 e^{\frac{\Delta E_g}{kT}} \left(e^{\frac{qV_{OC}}{kT}} - 1 \right)}. \tag{18}$$

If we compare the expressions for Δn and Δn_{OC}, as well as for the dark current (17) and photogeneration current (18), one sees that they coincide with each other, if we replace V by V_{OC} and I_D by I_L and also put R_S in (15) to zero.

This means that the solutions $I_D(V, R_{sh}, R_s)$ and $I_L(V_{OC}, R_{sh})$ are identical if $R_S = 0$. And $V_{OC}(\Delta n_{OC})$ can be found from (18):

$$V_{OC} = \frac{kT}{q} ln \left(\frac{(\Delta n_{OC} + n_0) \cdot \Delta n_{OC}}{n_{i0}(T)^2 e^{\frac{\Delta E_g}{kT}}} + 1 \right). \tag{19}$$

Multiplying current $I(V)$ on the applied voltage V, we get the SC generated power $P(V)$, and maximizing this using $\frac{dP}{dV}=0$ condition we find the voltage V_M at the point of maximum power. Substituting V_M in equation (12), we obtain the current I_M at the maximum power point. This allows calculating photoconversion efficiency η and the *I–V* fill-factor *FF* in the usual way. Note that in the approximation used, the short-circuit current I_{SC} value is a parameter, which should be defined from the experiment.

On the other hand, the short-circuit current in the textured silicon SCs can be calculated if the external quantum efficiency of the photocurrent $EQE(\lambda)$ is known. As it was shown in [12], for a number of high efficiency textured silicon SCs with *p-n* junctions and *HIT* elements, the external quantum yield in the long-wavelength region can be described by the following empirical formula:

$$EQE(\lambda) = [1 + b/(4 n_r(\lambda)^2 \cdot \alpha(\lambda) d)]^{-1}, \tag{20}$$

where b is a numerical coefficient larger than one. For the SCs considered, both $EQE(\lambda)$, the experimental dependence and their approximation by expression (20) were given in Fig. 1, The value b=4 leads to a good agreement of the experimental and calculated dependencies in the important long-wavelength region in the range from 800 to 1200 nm. Using this empirical formula, for the IBC SC considered the short-circuit photocurrent density J_L at AM 1.5 can be calculated by the formula

$$J_L(d,b) = q\left[\int_{\lambda_0}^{800} I_{AM1,5}(\lambda)EQE(\lambda)d\lambda + f\int_{800}^{\lambda_m} I_{AM1,5}(\lambda)EQE(\lambda,b)d\lambda\right], \quad (21)$$

where λ_0 = 300 nm, λ_m = 1200 nm, $I_{AM1.5}(\lambda)$ is the spectral density of the photon flux at AM 1.5, $EQE(\lambda,b)$ is determined by Eq. (20), and the coefficient $f \leq 1$. The f value is chosen that at λ = 800 nm the values $EQE(\lambda,b)$ and $IQE(\lambda,b)$ coincide. In this way the I_L dependence on the base thickness d can be found, which allows to optimize the SCs on the base thickness.

IV. THE RESULTS AND ANALYSIS

To validate the above theoretical approach developed and its application, we characterized experimentally the commercial textured silicon *p-n* junction SCs with a photoconversion efficiency η above 21%, which are manufactured by SunPower™. The SCs with rear contact metallization, have a photoactive area of 154.7 cm^2 and the base thickness d = 165 μm. Fig. 2 shows the dark *I–V* characteristic of one of the solar cells studied.

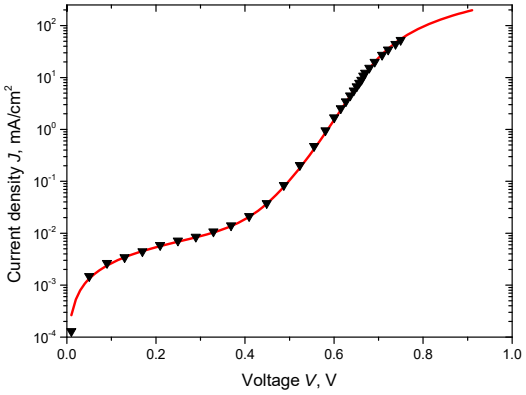

Fig. 2. Dark *I-V* characteristic of the SunPower™ solar cell. Triangles are the experimental values; the solid line is the theory.

To theoretically model dark *I–V* characteristics, it is necessary to find the recombination parameters, in particular τ_R and b_r, that determine the recombination rate in the SCR. When modeling the SCR recombination, we consider its Gaussian-like dependence of the distribution of the inverse life time in the SCR, as given by (11).

The above theoretical result has been compared to the experimental $J_D(V)$ dependence that we measured. The following parameters: n_0= 9·10^{14} cm^{-3}, d = 165 μm, τ_m = 1.3 · 10^{-5} s, x_m= 180 nm, σ = 50

nm, and b_r= 0.1 were obtained from the fit: the total rate of the surface recombination at a low excitation level S_{0s} is 5 cm/s. We assumed in the simulation that τ_{SRH} = 10 ms, which matched well this from [23].

Fig. 3 shows the theoretical $S_{sc}(\Delta n)$ dependence, plotted using the parameters obtained from the fit.

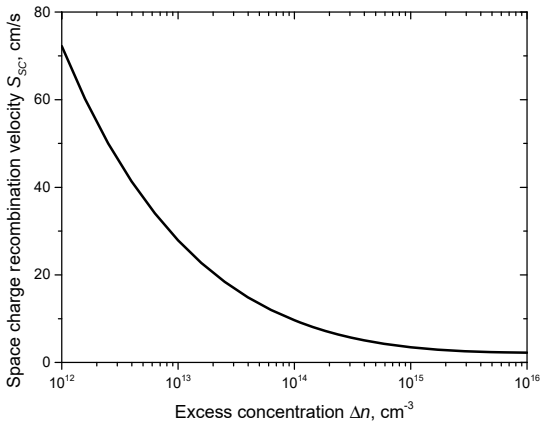

Fig. 3. Theoretical dependence of the recombination velocity in SCR on the excess concentration, $S_{SC}(\Delta n)$.

Fig. 4 shows the light *I–V* characteristic, measured at AM1.5, for the SunPower™ SC with the open circuit voltage V_{OC}= 0.692 V, and the short-circuit current density J_{SC} = 40.04 mA/cm^2. Experimental and calculated light *I–V* characteristics agree well when using the same components of the effective lifetime as for the dark *I–V* characteristics.

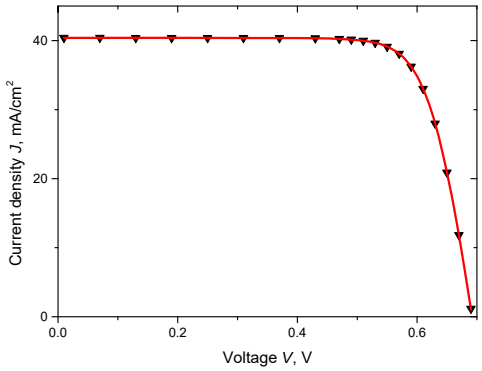

Fig. 4. Measured and calculated light *I–V* characteristics. Triangles are the experimental values; the solid line is from the theory.

Next, Fig. 5 shows the experimental and theoretical dependencies of $J_D(V)$ as well as $J_L(V_{OC})$ for the SC at temperature of 25°C. The figure demonstrates that when both V and V_{OC} is less than 0.62V the $J_D(V)$ and $J_L(V_{OC})$ graphs coincide. This is consistent with the analysis above

In contrast to similar dependencies, reported in the literature (see, for example, [4], [6]), these dependencies are both measured and calculated in a much wider range of J_L, including, in particular, the region of low photocurrent density J_L. Estimates show that at J_L <10^{-5}A/cm^2 the inequality $\frac{V_{OC}}{R_{sh}} > J_L$ holds. In the case when $J_L = 4 \cdot 10^{-2}$A/cm^2, compared to that J_L the $\frac{V_{OC}}{R_{sh}}$ value is two and a half orders of magnitude less and can be neglected in Eq. (17).

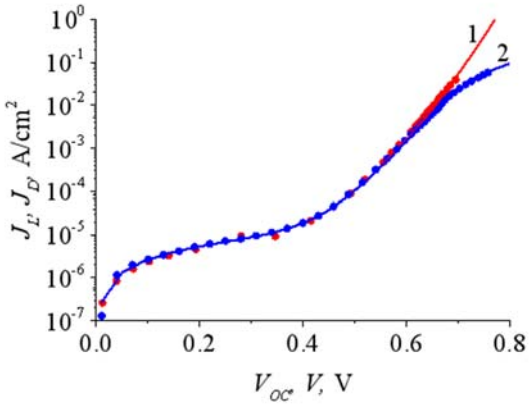

Fig. 5. Experimental dependencies of the short-circuit current J_L on the open-circuit voltage V_{OC} (red points) and of dark current J_D on the applied voltage V (blue points). Lines are the theoretical dependencies: 1 - $J_L(V_{OC})$, red line; 2 - $J_D(V)$, blue line.

The theoretical $J_L(V_{OC})$ dependence can be found from a joint solution of Eqs. (17) and (18) using the same parameters as for calculation of the dark I–V characteristic. As can be seen from Fig. 5, there is a good agreement between the experiment and the theory. A comparison between Figs. 2 and 5 also shows that when V and V_{OC} are less than 0.62 V, the solutions $J_D(V)$ and $J_L(V_{OC})$ coincide. This is consistent with the above analysis.

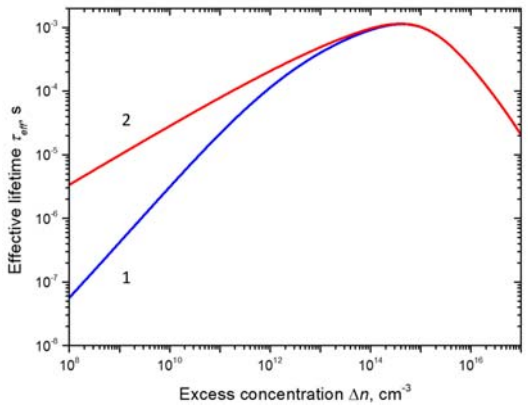

Fig. 6. Theoretical $\tau_{eff}(\Delta n)$ dependencies. Upper curve 1 (blue line) is calculated using Eq. (22), while the curve 2 above (red line) is from Eq. (23).

We plot the $\tau_{eff}(\Delta n_{OC})$ dependence in Fig. 6 using the expressions (22) and (23):

$$\tau_{eff1} = \left(\frac{J_L + \frac{V_{OC}}{R_{sh}}}{\Delta n_{OC} q d}\right)^{-1}, \qquad (22)$$

$$\tau_{eff2} = \left[\frac{1}{\tau_{SRH}} + \frac{1}{\tau_r(\Delta n_{OC})} + \frac{1}{\tau_{nr}(\Delta n_{OC})} + \frac{1}{\tau_{Auger}(\Delta n_{OC})} + \frac{S_{00s}}{d}\left(1 + \frac{\Delta n_{OC}}{n_0}\right) + \frac{A_B}{A_{SC}}\frac{S_{sc}}{d}\right]^{-1}. \qquad (23)$$

The two graphs 1 and 2 in Fig. 6 differ on whether the short-circuit current density component $\frac{V_{OC}}{R_{sh}}$ is included (curve 1) or neglected (curve 2). As can be seen from Fig. 6, at the right of the τ_{eff} maximum both curves depend on Δn_{OC} identically, while at the left of the maximum they deviate. Therefore, the $\frac{V_{OC}}{R_{sh}}$ component has to be included into consideration, as it is done for the accurate curve 1. However, further modeling in order to find the open circuit voltage V_{OC} and photoconversion efficiency η using the expression (19) for V_{OC} and η, shows that both dependencies provide the correct results. In particular, at S_{00s}= 5 cm/s the experimental and theoretical V_{OC} values coincide, while the experimental and calculated photoconversion efficiencies are also the same, η = 21.5% (R_s = 1.1 Ohm·cm^2 is chosen). As well, in this case the experimental and calculated *I–V* filling factors, equal to 87.7%, coincide.

Fig. 7 shows the calculated efficiency η dependence on the base doping level n_0. As can be seen from the figure, the maximum of $\eta(n_0)$ = 21.69% is reached at n_0= 5.5 · 10^{15} cm^{-3}, this differs from the experimental value by less than one percent.

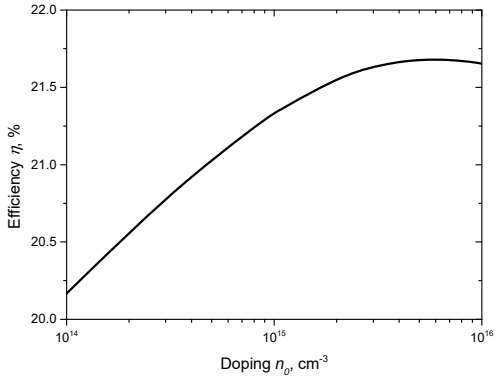

Fig. 7. Theoretical dependence of the photoconversion efficiency η on the base doping level n_0. Its maximum of 21.69% is achieved at $n_0 = 5.5 \cdot 10^{15}$ cm^{-3}

Using the expression (18), the coefficient b from the phenomenological formula (20) for $EQE(\lambda)$ in the long-wavelength range can be found and it equals to 4. Using $b = 4$, as well as the expression (19) for the base thickness d dependent short-circuit current, we can calculate the base thickness dependent photoconversion efficiency, which is shown in Fig. 8. As can be seen from the figure, the maximum η = 21.72% is reached at d = 750 μm, which is only one percent above the experimental value.

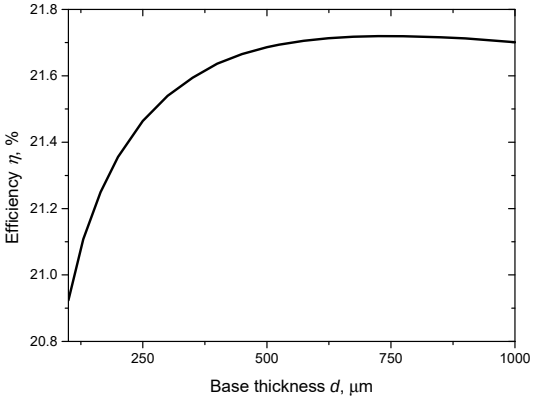

a.

Fig. 8. The photoconversion efficiency η dependence on the base thickness d. The efficiency maximum η = 21.72% is achieved at d = 750 μm.

The comparison of the experimental and theoretical results in Figs (2), (4), (6) clearly demonstrates a very good agreement and prove that formalism developed can be successfully used not to only better

understand the photoconversion mechanisms and its limiting factors in a wide class of the highly-efficient silicon-based textured SCs. More important is that this makes possible optimize the SCs in terms of their parameters.

V. CONCLUSIONS

We characterized experimentally the high efficiency commercial SunPower™ IBC SCs, measuring the open-circuit voltage V_{OC} dependent photocurrent density $J_{SC}(V_{OC})$ in a wide range of the densities, which allows extracting correct dependence of the total effective recombination lifetime $\tau_{eff}(\Delta n)$ on the excess concentration Δn. The measurements demonstrate that at $\Delta n < 4 \cdot 10^{14}$ cm^{-3} the lifetime τ_{eff} decreases with decreasing Δn, which indicates a significant effect of recombination in the SCR in the area with excess concentrations of electron-hole pairs. This is also evidenced by the dark *I–V* characteristics of the SCs under consideration.

To reproduce the experimental results theoretically, we proposed a comprehensive and physically transparent formalism to model and optimize the high efficiency textured silicon-based solar cells. Its application proves that the contribution of nonradiative exciton recombination, as a rule, exceeds the radiative recombination contribution and substantially affects the photoconversion efficiency, stronger than the gap narrowing effect.

The proposed approach allows to correctly model the short-circuit current and the efficiency of photoconversion in the highly efficient textured silicon solar cells. The formalism allows to self-consistently calculate such key SCs parameters as the short-circuit current density J_{SC}, open-circuit voltage V_{OC} and photoconversion efficiency η. Such calculations have been carried out for several SCs types, achieving very good agreements of the calculated characteristics with the experimental ones. This allows also to optimize the technologically important SCs base thickness and the doping level.

It is also shown that the recombination in SCR decreases the effective recombination time $\tau_{eff}(\Delta n)$ in the region of small Δn values.

We concluded from our analysis that the standard experimentally measured SCs characteristics, such as open circuit voltage V_{OC}, short circuit current density J_{SC}, fill factor *FF*, as well as the power P_m, voltage V_m, current density J_m at the maximum power point, junction saturation current density J_0, are usually not sufficient to comprehensively model and optimize the textured silicon SCs. To carry out such modeling and optimization, the experimental dependence $\tau_{eff}(\Delta n)$, measured on the ready-made SCs, or the experimental dark *I–V* characteristics are also required.

ACKNOWLEDGMENT

This work was partially supported (V. Kostylyov, V. Vlasiuk, and O.Ya. Olikh) by National Research Foundation of Ukraine by the state budget finance (project 2020.02/0036 “Development of physical base of both acoustically controlled modification and machine learning–oriented characterization for silicon solar cells”).

AVAILABILITY OF DATA

The data that support the findings of this study are available from the corresponding authors upon reasonable request.

REFERENCES

[1] Fraunhofer Institute for Solar Energy Systems, *Photovoltaics Report;* *https://www.ise.fraunhofer.de/content/dam/ise/de/documents/publications/studies/Photovoltaics-Report.pdf*, 2021).

[2] J. Liu, Y. Yao, S. Xiao, and X. Gu, J. Phys. D **51**, 123001 (2018).

[3] M. Green, E. Dunlop, J. Hohl-Ebinger, M. Yoshita, N. Kopidakis, and X. Hao, Prog Photovoltaics Res Appl **29**, 3 (2021).

[4] K. Yoshikawa, H. Kawasaki, W. Yoshida, T. Irie, K. Konishi, K. Nakano, T. Uto, D. Adachi, M. Kanematsu, H. Uzu*, et al*, Nature Energy **2**, 17032 (2017).

[5] A. Sachenko, V. Kostylyov, I. Sokolovskyi, and M. Evstigneev, IEEE Journal of Photovoltaics **10**, 63 (2020).

[6] K. Yoshikawa, W. Yoshida, T. Irie, H. Kawasaki, K. Konishi, H. Ishibashi, T. Asatani, D. Adachi, M. Kanematsu, H. Uzu*, et al*, Solar Energy Mater. Solar Cells **173**, 37 (2017).

[7] A. Augusto, J. Karas, P. Balaji, S. G. Bowden, and R. R. King, J. Mater. Chem. A **8**, 16599 (2020).

[8] A. V. Sachenko, V. P. Kostylyov, V. M. Vlasiuk, I. O. Sokolovskyi, and M. Evstigneev, J Lumin **183**, 299 (2017).

[9] A. V. Sachenko, V. P. Kostylyov, V. M. Vlasiuk, R. M. Korkishko, I. O. Sokolovs’kyi, and V. V. Chernenko, Ukr. J. Phys. **61**, 917 (2016).

[10] See, e.g., https://www.pvlighthouse.com.au/simulation-programs for the solar cell simulation software.

[11] A. Sachenko, V. Kostylyov, I. Sokolovskyi, B. Arzhang, and M. Evstigneev, 2020 47th IEEE Photovoltaic Specialists Conference (PVSC), 0715 (2020).

[12] A. V. Sachenko, V. P. Kostylyov, A. V. Bobyl, V. N. Vlasyuk, I. O. Sokolovskyi, G. A. Konoplev, E. I. Terukov, M. Z. Shvarts, and M. Evstigneev, Technical Physics Letters **44**, 873 (2018).

[13] M. A. Green, Prog. Photovolt: Res. Appl. **10**, 235 (2002).

[14] A. V. Sachenko, Y. V. Kryuchenko, V. P. Kostylyov, A. V. Bobyl, E. I. Terukov, S. N. Abolmasov, A. S. Abramov, D. A. Andronikov, M. Z. Shvarts, I. O. Sokolovskyi*, et al*, J. Appl. Phys. **119**, 225702 (2016).

[15] A. Sachenko, V. Kostylyov, V. Vlasiuk, I. Sokolovskyi, and M. Evstigneev, in *2020 47th IEEE Photovoltaic Specialists Conference (PVSC)*, 2020), p. 0719.

[16] T. Tiedje, E. Yablonovitch, G. D. Cody, and B. G. Brooks, IEEE Trans. Electron Devices **31**, 711 (1984).

[17] T. Niewelt, A. Richter, T. C. Kho, N. E. Grant, R. S. Bonilla, B. Steinhauser, J. -. Polzin, F. Feldmann, M. Hermle, J. D. Murphy*, et al*, Solar Energy Mater. Solar Cells **185**, 252 (2018).

[18] A. Richter, S. W. Glunz, F. Werner, J. Schmidt, and A. Cuevas, Phys.Rev.B **86**, 165202 (2012).

[19] A. P. Gorban, V. P. Kostylyov, A. V. Sachenko, A. A. Serba, and I. O. Sokolovsky, Ukr. J. Phys. **51**, 598 (2006).

[20] A. V. Sachenko, V. P. Kostylyov, I. O. Sokolovskyi, A. V. Bobyl', V. N. Verbitskii, E. I. Terukov, and M. Z. Shvarts, Technical Physics Letters **43**, 152 (2017).

[21] C. Sah, R. N. Noyce, and W. Shockley, Proceedings of the IRE **45**, 1228 (1957).

[22] A. B. Sproul and M. A. Green, J. Appl. Phys. **73**, 1214 (1993).

[23] D. D. Smith, G. Reich, M. Baldrias, M. Reich, N. Boitnott, and G. Bunea, "Silicon solar cells with total area efficiency above 25%" in Photovoltaic Specialists Conference (PVSC), 2016 IEEE 43rd, 3351–3355, IEEE. (2016) (2016).